

Proceeding Paper

# Synthesis and Application of Magnesium-Based Nanoparticles for the Photocatalytic Degradation of Methylene Blue in Aqueous Solutions: Optimization and Kinetic Modeling <sup>†</sup>

Khumbolake Faith Ngulube <sup>1,\*</sup>, Mahmoud Nasr <sup>1,2</sup>, Manabu Fujii <sup>3</sup> and Amal Abdelhaleem <sup>1</sup>

<sup>1</sup> Environmental Engineering Department, Egypt-Japan University of Science and Technology (E-JUST), Alexandria 21934, Egypt; mahmoud.nasr@ejust.edu.eg (M.N.); amal.elsonbaty@ejust.edu.eg (A.A.)

<sup>2</sup> Sanitary Engineering Department, Faculty of Engineering, Alexandria University, Alexandria 21544, Egypt

<sup>3</sup> Department of Civil and Environmental Engineering, Tokyo Institute of Technology, Tokyo 152-8552, Japan; fujii.m.ah@m.titech.ac.jp

\* Correspondence: khumbolake.ngulube@ejust.edu.eg

† Presented at the 2nd International Electronic Conference on Processes: Process Engineering—Current State and Future Trends (ECP 2023), 17–31 May 2023; Available online: <https://ecp2023.sciforum.net/>.

**Abstract:** Heterogeneous photocatalysis has been studied with various semiconductor materials for the efficient degradation of various water pollutants; however, there is the challenge of wide-bandgap photocatalyst materials, which limits their application under visible-light irradiation. Herein, a ZnO@MgO core–shell nanocomposite was synthesized using co-precipitation and applied to the photocatalytic degradation of MB dye under visible-light irradiation. MB degradation was optimized using the response surface methodology, resulting in 95.948% and ≈91% predicted and actual MB removals, respectively, at a 10 mg/L MB concentration, 1000 mg/L catalyst dose, pH 10, and time of 115.7 min. The degradation kinetics were studied, and it was found that the degradation followed pseudo-first-order kinetics with a rate constant of  $k = 0.07593 \text{ min}^{-1}$ . A cost–benefit analysis was undertaken, and the operating costs were estimated based on the optimized conditions at \$7.6/m<sup>3</sup> with a payback period of 3.2 years.



**Citation:** Ngulube, K.F.; Nasr, M.; Fujii, M.; Abdelhaleem, A. Synthesis and Application of Magnesium-Based Nanoparticles for the Photocatalytic Degradation of Methylene Blue in Aqueous Solutions: Optimization and Kinetic Modeling. *Eng. Proc.* **2023**, *37*, 75. <https://doi.org/10.3390/ECP2023-14636>

Academic Editor: Antoni Sánchez

Published: 17 May 2023



**Copyright:** © 2023 by the authors. Licensee MDPI, Basel, Switzerland. This article is an open access article distributed under the terms and conditions of the Creative Commons Attribution (CC BY) license (<https://creativecommons.org/licenses/by/4.0/>).

## 1. Introduction

Methylene blue (MB), commonly used in the textile industry, is a heterocyclic aromatic basic cationic dye that is highly soluble in water and forms stable solutions at room temperature. Therefore, its release into the environment has harmful effects on aquatic and human life. Its exposure in high concentrations could result in respiratory issues, abdominal disorders, blindness, and mental disorders, amongst others [1]. Aquatic life is not spared because MB causes a reduction in sunlight penetration into the marine environment [2]. This slows down the photosynthetic processes of aquatic plants, resulting in low dissolved oxygen levels, ultimately killing aquatic life and affecting the marine ecosystem's balance. Hence, it is of great importance that the wastewater contaminated by MB is adequately treated to prevent its exposure to the environment.

Conventional treatment techniques, such as adsorption, phytoremediation, coagulation/flocculation, and others, have been applied for the removal of MB from aqueous solutions. Due to the stable nature of MB, these have shown shortcomings in terms of their viability, impact on the environment, and effectiveness [3]. Therefore, advanced treatment techniques, such as advanced oxidation processes (AOPs), are being studied for the efficient removal of MB.

Heterogeneous photocatalysis is one of the most efficient AOPs that can degrade organic pollutants such as MB by generating reactive oxygen species (ROS), such as  $\cdot\text{OH}$ ,

from a series of oxidation and reduction reactions. ROS repeatedly attack and degrade MB by converting it into simpler molecules, such as  $\text{CO}_2$  and  $\text{H}_2\text{O}$ ; this sequence of reactions can take place at standard temperatures and pressures [4]. This technique does not generate large amounts of sludge, the photocatalyst material can be cheap, non-toxic, and reusable [5], and the reaction rates are relatively high [6]. Several semiconductor materials, such as  $\text{ZnO}$  and  $\text{MgO}$ , have been studied as photocatalysts and have displayed reasonable photocatalytic activity. However, there is still the need to identify photocatalyst materials that can display superior activity.

In this study, a  $\text{ZnO}@\text{MgO}$  core–shell nanocomposite material was synthesized, characterized, and applied to the photocatalytic degradation of MB under simulated solar UV-visible-light irradiation. The process was optimized using response surface methodology (RSM), and the resulting optimized conditions were used to carry out an economic analysis. To the best of our knowledge, there have been no published papers that have synthesized and applied this material.

## 2. Materials and Methods

### 2.1. Materials

Magnesium chloride hexahydrate ( $\text{MgCl}_2 \cdot 6\text{H}_2\text{O}$ ) (99%) was purchased from the tekkim kimya group of companies (Turkey), zinc sulfate heptahydrate ( $\text{ZnSO}_4 \cdot 7\text{H}_2\text{O}$ ) was purchased from the el nasr pharmaceutical chemicals company in Egypt, purified sodium hydroxide pellets ( $\text{NaOH}$ ) (97%) were purchased from SD fine—chem limited (India), the sulfuric acid ( $\text{H}_2\text{SO}_4$ ) (97%) and methanol ( $\text{CH}_3\text{OH}$ ) (99.8%) were purchased from piochem in Egypt, and the methylene blue powder (MB) (99%) was purchased from the alpha chemical group, Egypt.

### 2.2. Preparation of Methylene Blue Solution

A 500 ppm stock solution of MB dye was prepared by dissolving 500 mg of MB dye powder into 1 L of distilled water. This stock solution was stored in a cool, dry environment and then diluted to the desired concentrations for use in the experimental runs.

### 2.3. Photocatalyst Synthesis

$\text{MgO}$  nanoparticles were synthesized using a 0.5 M precursor solution of  $\text{MgCl}_2 \cdot 6\text{H}_2\text{O}$  following the method used by the authors of [7]. The obtained dried powder was then calcined in a muffle furnace at 800 °C for 3 h to obtain the  $\text{MgO}$  nanoparticles.

To synthesize the  $\text{ZnO}@\text{MgO}$  core–shell nanocomposite, the as-synthesized  $\text{MgO}$  nanoparticles were dispersed into a solution of  $\text{ZnSO}_4 \cdot 7\text{H}_2\text{O}$  and stirred vigorously to keep the  $\text{MgO}$  nanoparticles in suspension. The synthesis steps proceeded as in the case of  $\text{MgO}$ ; however, the obtained white powder was calcined at 350 °C for 3 h to obtain the  $\text{ZnO}@\text{MgO}$  core–shell nanocomposite. The synthesis procedures are summarized in Figure S1.

### 2.4. Characterization

A UV-Vis diffuse reflectance spectrum (UV-Vis DRS, Jasco v-570 spectrometer, Jasco Inc., Tokyo, Japan) analysis was carried out in order to determine the optical bandgap energy of the catalysts. The MB dye concentration was measured using a UV spectrophotometer (Jasco V-630 spectrophotometer, Jasco Inc., Tokyo, Japan) set at a wavelength of 664 nm.

### 2.5. Photocatalytic Degradation

#### 2.5.1. Degradation Experiments

The photocatalytic degradation experiments involved the dilution of the MB stock solution to the desired concentration and adjusting the pH by adding  $\text{NaOH}$  or  $\text{H}_2\text{SO}_4$  until the desired pH was achieved. The catalyst was then added into the MB solution and placed in the reactor under constant stirring in the dark for 1 h to allow for an adsorption–desorption equilibrium. After an adsorption–desorption equilibrium was achieved, a

2 mL sample was extracted and centrifuged to separate the catalyst from the solution and the concentration;  $C_0$  was measured. The light in the reactor was switched on and photocatalytic degradation was allowed to proceed for the desired amount of time,  $t$ , after which another 2 mL sample was extracted and the final MB concentration,  $C_t$ , was measured. MB removal,  $R\%$ , was calculated using the formula given by Equation (1):

$$R\% = \frac{C_0 - C_t}{C_0} \times 100 \quad (1)$$

#### 2.5.2. Statistical Analysis

The experimental design and optimization of parameters were carried out with design expert 13 software using a Box–Behnken design (BBD). It was used to study the effects of four selected independent variables, A (dye concentration), B (catalyst dose), C (pH), and D (time), on MB dye removal. The BBD generated a total of 29 experimental runs comprising five center points. A second-order polynomial, given by Equation (2), was used to study the effects of the variables on the removal of MB and to show how each of the variables affect each other:

$$y = c_0 + \sum_{i=1}^n c_i x_i + \sum_{i=1}^{n-1} \sum_{j=i+1}^n c_{ij} x_i x_j + \sum_{i=1}^n c_{ii} x_i^2, \quad (2)$$

where  $y$  is the MB removal,  $n$  is the number of independent variables,  $c_0$  is a constant,  $c_i$ ,  $c_{ij}$ , and  $c_{ii}$  are the first-order constant, quadratic, and linear interaction coefficients, respectively,  $x_i$  and  $x_j$  are independent variables, and  $x_i^2$  is a square effect.

To verify the adequacy of the generated model and each of the independent variables, an analysis of variables (ANOVA) was performed, and the significance of each parameter was denoted by a  $p$ -value less than 0.05. The model significance was also verified using the coefficient of determination ( $R^2$ ) values. Once the model was verified, optimization of parameters was carried out using numerical optimization, and the degradation kinetics were studied.

### 3. Results and Discussion

#### 3.1. UV-Vis DRS

Figure 1a shows the absorbance spectrum of ZnO@MgO core–shell nanocomposite. Moreover, an indirect Tauc plot [8] was drawn as shown in Figure 1b.

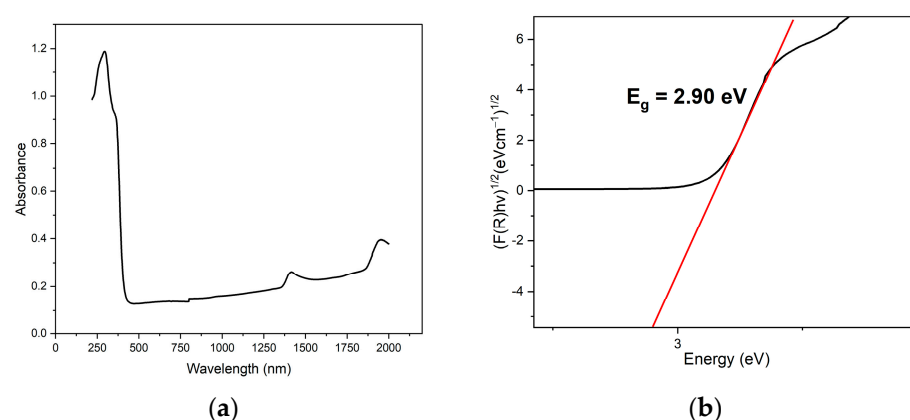


**Figure 1.** (a) Absorbance spectrum and (b) Tauc plot of the ZnO@MgO core–shell nanocomposite.

The plot was derived from the UV-Vis DRS analysis results using the equation given by Equation (3):

$$[F(R)hv]^n = A(hv - E_g), \quad (3)$$

where  $F(R)$ ,  $hv$ ,  $A$ , and  $E_g$  are the Kubelka–Munk function, incident photon energy, proportionality constant, and bandgap energy, respectively, and  $n$  is  $1/2$ . The extrapolation of

the linear section of the graph revealed that the optical bandgap energy of the ZnO@MgO core–shell nanocomposite was 2.90 eV. The theoretical bandgap energy of pure ZnO has been identified in the literature to be around 3.33 eV [9], whereas that of pure MgO has been identified as 4.8 eV [10]. The reduction in the energy bandgap of the nanocomposite shows successful bandgap narrowing by the core–shell combination of the two materials. The reduced bandgap can facilitate better electron excitation within the visible-light irradiation range (400–800 nm) compared with the pure ZnO and MgO separately.

### 3.2. Optimization, Validation, and Kinetics

An ANOVA was carried out (Table S1) and the model generated had a  $p$ -value < 0.05 as well as relatively high adjusted and predicted  $R^2$  values of 0.9939 and 0.9826, respectively, which had a difference of less than 0.2. This validated the generated model as significant and suitable to be used for further analyses. The analysis also showed that all of the four independent variables were significant to the degradation of the MB dye.

A second-order polynomial governing MB removal based on the independent variables was generated as shown in Equation (4):

$$\begin{aligned} R\% = 9.56 - 29.84A + 2.84B + 13.18C + 2.71D - 1.99AB - 14.05AC - 2AD + 6.05BC + 1.37BD + \\ 8.72CD + 19.56A^2 + 1.43B^2 - 1.40C^2 + 1.01D^2, \end{aligned} \quad (4)$$

Numerical optimization of the variables was carried out by maximizing the desired MB removal and reducing the reaction time. The analysis generated 100 possible optimized conditions, of which the one selected displayed an MB removal of 95.948% in 115.7 min for a dye concentration of 10 mg/L, catalyst dose of 1000 mg/L, and pH 10. The generated contour plots showing the interactions of the independent variables are shown in Figure S2.

A validation run was carried out at the optimized conditions and a removal efficiency of 90.858% was achieved. Samples of 2 mL were extracted and analyzed at 15 min intervals, and the  $C/C_0$  curve was plotted as shown in Figure 2a. The degradation kinetics were then studied in order to determine the reaction rate constant, where the MB removal was checked for fitness with zero-order, half-order, first-order, and second-order degradation kinetics.

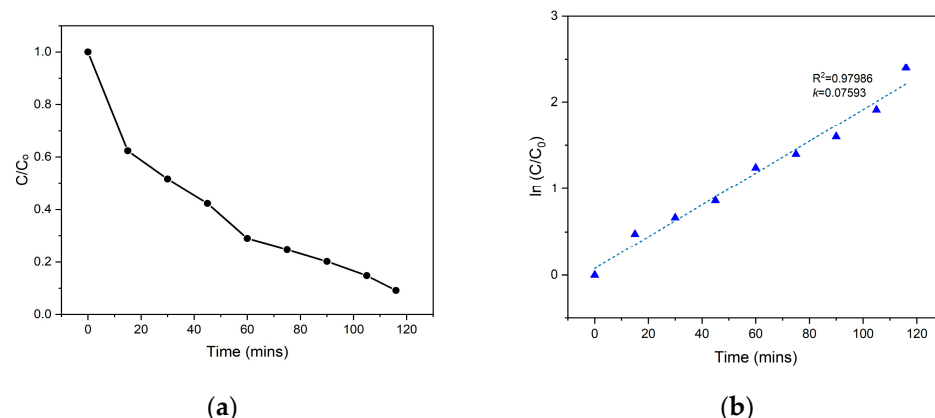


**Figure 2.** (a) MB removal, (b) pseudo-first-order degradation kinetics (reaction conditions: MB concentration = 10 mg/L, catalyst dose  $\approx$  1000 mg/L, pH = 10, and time = 115.7 min).

The reaction rate constant(s),  $k$ , were calculated as the slopes of the zero-order, half-order, first-order, and second-order kinetics curves given by the equations in Table S2 [11].

The  $R^2$  values of each model showed that the MB removal in this study was compatible with pseudo-first-order degradation kinetics (Figure 2b) with a reaction rate constant of  $0.07593 \text{ min}^{-1}$ .

### 3.3. Effects of Operational Parameters

The effect of the independent variables on the removal of the MB dye was studied and the graphs generated are shown in Figure S3.

#### 3.3.1. Effect of Dye Concentration

The effect change in MB concentration was investigated by varying the dye concentration from 10 to 100 mg/L (Figure S3a). As the MB concentration was increased, the removal efficiency decreased. The decrease in the removal efficiency could be a result of the blocking of active sites on the photocatalyst surface with increased dye concentrations [12], which results in reduced interactions between photons and active sites and ultimately limits the generation of ROS for MB degradation. Another reason for this reduction is that when the dye concentration is high, light penetration to the photocatalyst surface is reduced [13]. Photon energy will be absorbed by the dye molecules instead of the catalyst material. Additionally, the newly generated intermediates that will be formed during the photocatalytic reaction will compete with the parent dye molecules for the reactive radicals.

#### 3.3.2. Effect of Catalyst Dose

In order to study the effect of catalyst dosage on the photocatalytic degradation of MB dye, the concentration of ZnO@MgO in the degradation experiments was varied from 100 to 1000 mg/L (Figure S3b). It was observed that the removal efficiency increased as the catalyst dosage was increased from 100 mg/L to 1000 mg/L. The increment in removal efficiency can be attributed to the increased number of active sites at higher catalyst dosages. This increase allows for more catalyst–photon interactions, followed by the generation of more ROS to degrade the MB dye [12].

#### 3.3.3. Effect of pH

The effect of pH on the photocatalytic removal of the dye was studied at pH ranges of 3 to 10 (Figure S3c). The results showed that the removal efficiencies improved with an increase in the solution pH value. The trend displayed is acceptable given that MB dye is a cationic dye (positively charged), and when the solution pH exceeds the point of zero charge (PZC) pH of 10.44 (Figure S4) the catalyst surface charge becomes negative [14]. When the catalyst was added to a neutral MB dye solution the pH increased to about 11, and when the initial MB concentration is set to 10 the solution pH would further increase to about 11.55, making the surface charge of the catalyst negative. The opposite charge of the catalyst to the MB dye molecules will result in greater attraction of MB to the catalyst surface. This attraction will increase MB–ROS interactions, resulting in higher removal efficiencies.

#### 3.3.4. Effect of Time

The effect of time on MB removal was studied by varying the time between 60 and 180 min (Figure S3d). It was observed that MB removal and time displayed a directly proportional relationship. Further increases in the reaction time caused an obvious increase in the MB removal efficiency. This is due to prolonged contact time [15] between the generated ROS on the photocatalyst surface and the MB dye.

### 3.4. Economic Evaluation

In order to estimate the feasibility of the up-scale synthesis and application of the ZnO@MgO core–shell nanocomposite for dye removal, an economic analysis was carried out where the capital costs, operating costs, and possible revenues were estimated as shown in Table S3 based on the optimized parameters of the lab experiments. The analysis assumes a daily wastewater inflow of 80 m<sup>3</sup>, which is suitable for a roughly medium-sized treatment plant.

The capital costs included the costs of the photocatalytic reactor and all its components, catalyst synthesis apparatus, plant infrastructure construction costs, contractor charges,

and contingencies calculated using the equation given in Table S4. The total capital costs were then estimated to be about USD 2,941,149.22.

The operational costs were also estimated and comprised expenses such as electricity, the cost of chemicals, water bills, statutory obligations such as taxes and workers' salaries, and equipment repair as well as maintenance costs. The total annual operational cost estimate amounted to USD 182,443.56, which gave a running cost of USD 7.6/m<sup>3</sup> of influent water. The possible revenues identified were the removal of dye from the water, the sale of the synthesized catalyst material, and the reuse of the treated effluent for on-site applications. The estimate of the total revenues was USD 1,097,416.73. Finally, the capital costs, operational costs, and revenues were used to derive the payback period, and it was estimated to be 3.2 years.

**Supplementary Materials:** The following supporting information can be downloaded at: <https://www.mdpi.com/article/10.3390/ECP2023-14636/s1>, Figure S1: Catalyst synthesis procedure; Figure S2: Interaction of parameters towards MB removal; Figure S3: Effect of operational parameters on MB removal: (a) effect of dye concentration; (b) effect of catalyst dose; (c) effect of pH; and (d) effect of time; Figure S4: PZC of the core–shell nanocomposite; Table S1: ANOVA table; Table S2: Equations governing the kinetic modeling; Table S3: Cost–benefit analysis; Table S4: Capital cost estimation formulae. References [16–18] are cited in the supplementary materials.

**Author Contributions:** Conceptualization, K.F.N., M.N., and A.A.; methodology, K.F.N.; software, M.N.; validation, K.F.N.; formal analysis, K.F.N.; investigation, K.F.N.; resources, M.N., A.A., and M.F.; data curation, K.F.N.; writing—original draft preparation, K.F.N.; writing—review and editing, K.F.N., M.N., and A.A.; visualization, K.F.N.; supervision, M.N., A.A., and M.F.; project administration, M.N. and A.A. All authors have read and agreed to the published version of the manuscript.

**Funding:** This research received no external funding.

**Institutional Review Board Statement:** Not applicable.

**Informed Consent Statement:** Not applicable.

**Data Availability Statement:** The data presented in this study are available upon request from the corresponding author.

**Acknowledgments:** The authors wish to acknowledge TICAD 7 for the scholarship of the researcher as well as JICA and E-JUST for all of the equipment used throughout the research.

**Conflicts of Interest:** The authors declare no conflict of interest.

## References

1. Cusioli, L.F.; Quesada, H.B.; Baptista, A.T.A.; Gomes, R.G.; Bergamasco, R. Soybean hulls as a low-cost biosorbent for removal of methylene blue contaminant. *Environ. Prog. Sustain. Energy* **2020**, *39*, e13328. [[CrossRef](#)]
2. Ebi Ebi, O.; Falilat Taiwo, A.; Tunde Folorunsho, A. Kinetic Modelling of the Biosorption of Methylene Blue onto Wild Melon (*Lagenaria sphaerica*). *Am. J. Chem. Eng.* **2018**, *6*, 126–134. [[CrossRef](#)]
3. Crini, G.; Lichtfouse, E. Advantages and disadvantages of techniques used for wastewater treatment. *Environ. Chem. Lett.* **2019**, *17*, 145–155. [[CrossRef](#)]
4. Ahmed, S.N.; Haider, W. Heterogeneous photocatalysis and its potential applications in water and wastewater treatment: A review. *Nanotechnology* **2018**, *29*, 342001. [[CrossRef](#)] [[PubMed](#)]
5. Karim, M.A.H.; Aziz, K.H.H.; Omer, K.M.; Salih, Y.M.; Mustafa, F.; Rahman, K.O.; Mohammad, Y. Degradation of aqueous organic dye pollutants by heterogeneous photo-assisted Fenton-like process using natural mineral activator: Parameter optimization and degradation kinetics. *IOP Conf. Ser. Earth Environ. Sci.* **2021**, *958*, 012011. [[CrossRef](#)]
6. Advanced Oxidation Processes (AOP) | Spartan. Spartan Water Treatment. Available online: <https://spartanwatertreatment.com/advanced-oxidation-processes/> (accessed on 19 March 2023).
7. Rao, K.G.; Ashok, C.H.; Rao, K.V.; Chakra, C.H.S. Structural properties of MgO Nanoparticles: Synthesized by Co-Precipitation Technique Structural properties of MgO Nanoparticles: Synthesized by Co-Precipitation Technique. *Int. J. Sci. Res.* **2014**, *3*, 43–46.
8. Makuła, P.; Pacia, M.; Macyk, W. How To Correctly Determine the Band Gap Energy of Modified Semiconductor Photocatalysts Based on UV-Vis Spectra. *J. Phys. Chem. Lett.* **2018**, *9*, 6814–6817. [[CrossRef](#)] [[PubMed](#)]
9. Kamarulzaman, N.; Kasim, M.F.; Rusdi, R. Band Gap Narrowing and Widening of ZnO Nanostructures and Doped Materials. *Nanoscale Res. Lett.* **2015**, *10*, 346. [[CrossRef](#)] [[PubMed](#)]

10. Almontasser, A.; Parveen, A.; Azam, A. Synthesis, Characterization and antibacterial activity of Magnesium Oxide ( $MgO$ ) nanoparticles. *IOP Conf. Ser. Mater. Sci. Eng.* **2019**, *577*, 012051. [[CrossRef](#)]
11. Mensah, K.; Samy, M.; Ezz, H.; Elkady, M.; Shokry, H. Utilization of iron waste from steel industries in persulfate activation for effective degradation of dye solutions. *J. Environ. Manag.* **2022**, *314*, 115108. [[CrossRef](#)] [[PubMed](#)]
12. Sadeghi, M.; Heydari, M.; Javanbakht, V. Photocatalytic and photo-fenton processes by magnetic nanophotocatalysts for efficient dye removal. *J. Mater. Sci. Mater. Electron.* **2021**, *32*, 5065–5081. [[CrossRef](#)]
13. Akpan, U.G.; Hameed, B.H. Parameters affecting the photocatalytic degradation of dyes using  $TiO_2$ -based photocatalysts: A review. *J. Hazard. Mater.* **2009**, *170*, 520–529. [[CrossRef](#)] [[PubMed](#)]
14. Alkaim, A.; Aljeboree, A.; Alrazaq, N.A.; Jaafer, S.; Hussein, F.; Lilo, A.J. Effect of pH on Adsorption and Photocatalytic Degradation Efficiency of Different Catalysts on Removal of Methylene Blue. *Asian J. Chem.* **2014**, *26*, 8445–8448. [[CrossRef](#)]
15. Kumar, A.; Pandey, G. The photocatalytic degradation of Methyl Green in presence of Visible light with photoactive Ni 0.10:La 0.05: $TiO_2$  nanocomposites. *IOSR J. Appl. Chem.* **2017**, *10*, 31–44. [[CrossRef](#)]
16. Munawar, T.; Mukhtar, F.; Yasmeen, S.; Naveed-ur-Rehman, M.; Nadeem, M.S.; Riaz, M.; Mansoor, M.; Iqbal, F. Sunlight-induced photocatalytic degradation of various dyes and bacterial inactivation using  $CuO$ – $MgO$ – $ZnO$  nanocomposite. *Environ. Sci. Pollut. Res.* **2021**, *28*, 42243–42260. [[CrossRef](#)] [[PubMed](#)]
17. Vishwanathan, S.; Das, S. Glucose-mediated one-pot hydrothermal synthesis of hollow magnesium oxide-zinc oxide ( $MgO$ – $ZnO$ ) microspheres with enhanced natural sunlight photocatalytic activity. *Environ. Sci. Pollut. Res.* **2023**, *30*, 8512–8525. [[CrossRef](#)] [[PubMed](#)]
18. Revathi, V.; Karthik, K. Microwave assisted  $CdO$ – $ZnO$ – $MgO$  nanocomposite and its photocatalytic and antibacterial studies. *J. Mater. Sci. Mater. Electron.* **2018**, *29*, 18519–18530. [[CrossRef](#)]

**Disclaimer/Publisher's Note:** The statements, opinions and data contained in all publications are solely those of the individual author(s) and contributor(s) and not of MDPI and/or the editor(s). MDPI and/or the editor(s) disclaim responsibility for any injury to people or property resulting from any ideas, methods, instructions or products referred to in the content.